NANO LETTERS

2007
Vol. 7, No. 11
3305−3314

Active Nanodiamond Hydrogels for Chemotherapeutic Delivery

Houjin Huang,[†] Erik Pierstorff,[†] Eiji Osawa,[‡] and Dean Ho*[,†,§]

Departments of Biomedical and Mechanical Engineering, Robert R. McCormick School of Engineering and Applied Science, Northwestern University, Evanston, Illinois 60208, Nanocarbon Research Institute, Ltd., Chiba, Japan, and Robert H. Lurie Comprehensive Cancer Center, Feinberg School of Medicine, Northwestern University, Chicago, Illinois 60611

Received June 26, 2007; Revised Manuscript Received September 20, 2007

ABSTRACT

Nanodiamond materials can serve as highly versatile platforms for the controlled functionalization and delivery of a wide spectrum of therapeutic elements. In this work, doxorubicin hydrochloride (DOX), an apoptosis-inducing drug widely used in chemotherapy, was successfully applied toward the functionalization of nanodiamond materials (NDs, 2–8 nm) and introduced toward murine macrophages as well as human colorectal carcinoma cells with preserved efficacy. The adsorption of DOX onto the NDs and its *reversible release* were achieved by regulating Cl^- ion concentration, and the NDs were found to be able to efficiently ferry the drug inside living cells. Comprehensive bioassays were performed to assess and confirm the innate biocompatibility of the NDs, via real-time quantitative polymerase chain reaction (RT-PCR), and electrophoretic DNA fragmentation as well as MTT analysis confirmed the functional apoptosis-inducing mechanisms driven by the DOX-functionalized NDs. We extended the applicability of the DOX–ND composites toward a translational context, where MTT assays were performed on the HT-29 colon cancer cell line to assess DOX–ND induced cell death and ND-mediated chemotherapeutic sequestering for potential slow/sustained released capabilities. These and other medically relevant capabilities enabled by the NDs forge its strong potential as a therapeutically significant nanomaterial.

In clinical practice, the controlled delivery and release of pharmaceutical agents are often desirable, as the tailored dosing of many chemotherapeutics is vital toward the reduction of side effects and complications.[1,2] The utilization of nanoparticle-based vehicles as multifunctional, versatile, and biocompatible drug carriers would then serve as an ideal technology, as their significant advantages include the ability to target specific locations in the body, the reduction of the overall quantity of drug used at the active dosing site, and the potential to reduce the concentration of the drug at healthy/unaffected sites, resulting in fewer side effects that can significantly complicate the course of treatment.[3,4] From these advantageous aspects of nanoparticle-based chemotherapeutic delivery, a central capability that is then afforded is the prevention of generalized drug delivery, which is also a key mechanism for drug-induced medical treatment complications. For this and other purposes, in recent years, a considerable effort has been devoted to the design and synthesis of novel nanostructured materials with functional biological properties.[5−8] Among the various nanostructures being developed, carbon-based nanomaterials (e.g., fullerene and carbon nanotubes) are receiving much attention due to their remarkable physical, chemical, and biological properties.[9−17] For biological applications of nanocarbon materials, the scientific community has thus far been primarily focused on fullerenes and carbon nanotubes while their biocompatibility still receives continued assessment.[18−21] In particular, single-walled carbon nanotubes (SWNTs) have been recently explored as drug carriers,[22−26] as well as potential cancer cell-targeting/killing agents via infrared therapy.[27] However, they have also been previously shown to induce oxidative stress in human keratinocytes via the nuclear factor-κ B (NF-κB) transcription factor.[28]

Owing to its superior physical properties and biocompatibility, diamond-based nanostructures have emerged as alternative promising materials for biomedical applications such as diamond films for robust implant coatings and fluorescent nanodiamonds (NDs, 35 or 100 nm) as stable biomarkers.[29−31] Most of these applications are based on polycrystalline diamond films or diamond particles with a relative large grain size produced by chemical vapor deposition (CVD). On the other hand, ND powder-based particles with a much smaller size (<10 nm in diameter) can be readily

* Author to whom correspondence should be addressed. E-mail: d-ho@northwestern.edu. Telephone: (847) 467-0548. Fax: (847) 491-3915. Address: 2145 Sheridan Road, Evanston, IL 60208.

[†] Robert R. McCormick School of Engineering and Applied Science, Northwestern University.

[‡] Nanocarbon Research Institute, Ltd.

[§] Robert H. Lurie Comprehensive Cancer Center, Feinberg School of Medicine, Northwestern University.

10.1021/nl071521o CCC: $37.00
Published on Web 10/05/2007

generated by the detonation technique.[32] Recent progress in the dispersion of detonation NDs (2−8 nm) in aqueous media made by Osawa and colleagues has facilitated the use of NDs in physiological solutions.[33] Even more recently, the biocompatibility of detonation NDs has been assessed. Investigations of cell viability such as the MTT assay and luminescent ATP production showed that the NDs are not toxic to a variety of cell types.[34] Compared to other nanocarbon materials such as CNTs, which are toxic in some studies and naturally not water-soluble, it is thus envisaged that NDs can serve as an enhanced material for biomedical applications in physiological systems.[35] While detonation NDs have been used to adsorb proteins,[35−37] these studies do not address the broad range of drug-carrying applications of which this material can serve as a foundation. Furthermore, very critical testing of the innate biocompatibility of the NDs through *gene expression* studies was not considered in these earlier works even though preliminary studies of cell viability were examined.

In this context, we demonstrate in this work that NDs serve as efficient chemotherapeutic drug carriers. Doxorubicin hydrochloride (DOX), an apoptosis-inducing drug widely used in chemotherapy, was successfully coated on the NDs and/or embedded into the intervals of ND aggregates and introduced into living cells. The NDs were found to move inside the cells quickly and were capable of ferrying the drug inside living cells efficiently. In addition, comprehensive bioassays at the genetic level were performed to assess and confirm the innate biocompatibility of the NDs via RT-PCR, and electrophoretic studies of DNA fragmentation as well as MTT assays were applied toward the confirmation of functional apoptosis-inducing mechanisms enabled by the DOX-functionalized NDs. As such, this work demonstrates the potential that the NDs possess as a broad drug-functionalization platform technology for nanoscale medicine.

Characterization and Dispersion of Nanodiamonds. Nanodiamonds were generously supplied by NanoCarbon Research Institute Ltd. and were synthesized according to previously reported detonation techniques.[32−33] Before coating the drug onto the NDs, the chemical nature and purity of the material were investigated with Fourier transform infrared spectroscopy (FTIR, Thermal Nicolet, Nexus 870), Raman spectroscopy (Renishaw, inVia reflex microRaman, 514.5 nm laser), thermogravimetric analysis (TGA, TA instruments, SDT 2960), and transmission electron microscopy (TEM, Hitachi H-8100). From these characterization data, we ascertained the size of the NDs to be in the range of 2−8 nm, the purity of the NDs was over 90 wt %, and the NDs were heavily functionalized with hydrophilic functional groups such as −OH and −COOH on the surface.

Because the existence of the hydrophilic functional groups as well as the chemical linkage between ND particles in the as-received ND solids were largely disintegrated by stirred-media milling, a stable dispersion of the NDs in water ($\leq$100 μg/mL) could be readily achieved via mild ultrasonication (100 W, VWR 150D sonicator) for 30 min. Some polar aprotic solvents, such as dimethyl sulfoxide (DMSO) and *N*-methylpyrrolidone, have been confirmed to be superior solvents for dispersion of the NDs.[37]

Loading and Release of Doxorubicin Hydrochloride (DOX). Because the NDs are negatively charged (e.g., ND−COO^-) and doxorubicin ions (D−NH_3^+) are cationic, the interaction between the NDs and DOX appears to be straightforward. However, DOX ions are not easily adsorbed by the NDs due to the high aqueous dispersibility of both cations and anions. To observe the precipitation of DOX−ND composites from their aqueous suspension upon centrifuging, we found the addition of salt such as NaCl to be a necessary component of the loading process. As such, the salt was shown to be able to promote the adsorption of DOX onto the NDs. Without the addition of NaCl, less than 0.5 wt % of DOX could be adsorbed onto the NDs. In contrast, we achieved over 10 wt % adsorption of DOX on the NDs with the addition of NaCl (10 mg/mL). The function of the salt is schematically illustrated in Figure 1. The mechanism of salt-mediated adsorption of DOX onto the NDs can be explained by the observation that, in aqueous solution, without the addition of any other perturbation ions, the repulsive interaction of DOX−DOX and ND−ND is greater than the cohesive interaction of ND−DOX and thus an insignificant amount of DOX can be adsorbed onto the NDs. With the addition of NaCl, the increase of Cl^- ions may shift the balanced interactions toward the formation of DOX−ND complexes because cationic DOX is also balanced with anionic Cl^- ions.

As shown in Figure 2a, the disappearance of DOX characteristic peaks (e.g., 490 nm) and the formation of an orange-colored precipitate indicated the formation of DOX−ND composites upon the addition of NaCl. The inset shows photos of aqueous solutions of DOX (10 μg/mL), centrifuged ND/DOX/NaCl solution, and re-dispersed DOX−ND composite drug in water, respectively. Release of DOX from the NDs could be easily achieved by desalination, as seen in Figure 2b. To further examine the adsorption dynamics of DOX onto the NDs, we monitored the disappearance rate of DOX optical absorption, as shown in Figure 2c. An initial sharp increase followed by a gradual increase of DOX adsorbed to the ND surface (Figure 2d) can be understood by considering the aggregation nature of the NDs. Potential mechanistic explanations for the observed phenomenon include the notion that the potent DOX adsorption to the ND surfaces (Figure 3a,b) confirmed by TEM serve as an indicator that subsequent adsorption of DOX−ND composites comprehensively coated with DOX to neighboring and adjacent DOX−ND composites, also coated with DOX, would have generated aggregates with shielded DOX simply through the nature of the drug being buried toward the center of the aggregate structure. Optimized manufacturing of drug carriers would enable the fabrication of nanoparticles that support the integration of a drug that is both shielded as well as adsorbed to the interior of the carrier to prevent both systemic cytotoxicity or overelution through both drug shielding from unintended tissue exposure, as well as prevention of generalized activity through drug leakage, where the drug adsorption would serve as a sequestering

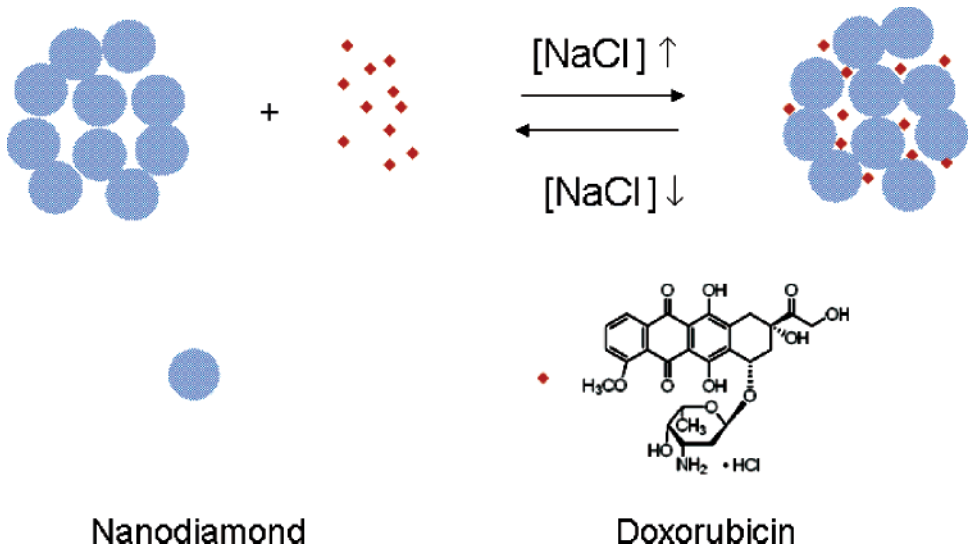

Figure 1. Schematic drawing of NaCl-mediated loading and release of doxorubicin hydrochloride. The addition of the salt induces functionalization of the drug onto the nanodiamond aggregate surface. Salt removal drives drug release. This mild switching process is amenable toward medically relevant processes.

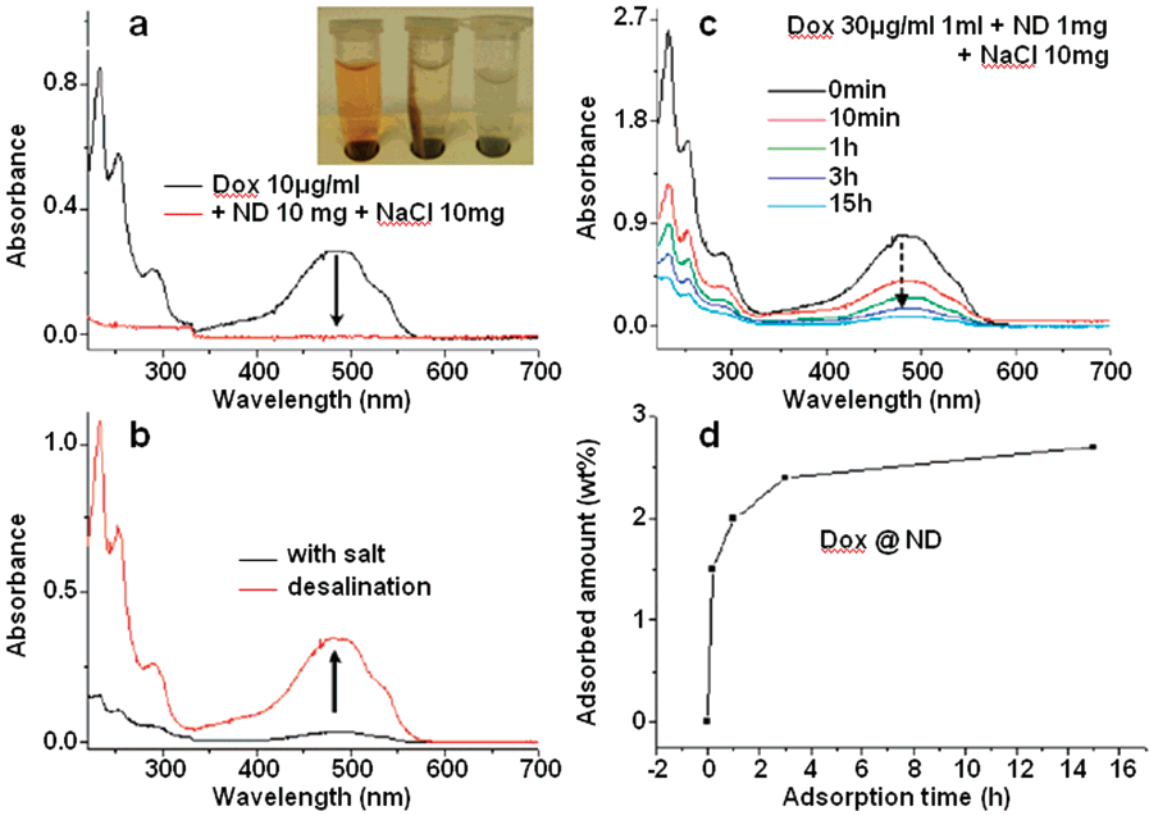

Figure 2. (a) UV−vis spectra of DOX before and after addition of nanodiamonds and NaCl. DOX (10 μg/mL) was completely removed from solution by the addition of NDs (10 mg) and NaCl (10 mg) followed by centrifuging at 10 000*g*. The inset shows aqueous solution of DOX (10 μg/mL), centrifuged ND/DOX/NaCl solution, and redispersed ND/DOX composite drug in water. (b) UV−vis spectra show that desalination results in release of DOX from NDs in which ~1.0 wt % of DOX has already been adsorbed. Desalination was performed by partial exchange of the salty supernatant with pure water. To further examine and confirm the effect of NaCl on the interfacing of DOX with the NDs, the gradual adsorption of the DOX on NDs was monitored using UV−vis spectrophotometry. (c) Gradual increase in DOX adsorption to the ND surface over time mediated by the presence of NaCl shown by the disappearance of free floating DOX from solution and interaction with the NDs. (d) Gradual increase in weight % of the DOX adsorbed to the ND surface.

function as well. For the purposes of this study, we focused on the demonstration of DOX adsorption and desorption from ND aggregates as an elucidative work to characterize novel material routes for therapeutic delivery, while ongoing work addresses the optimization of chemotherapeutic loading and transfer. As such, these observed phenomena may then have enabled a slow-release/delamination element of the ND carrier system. The adsorption of the drug to the NDs can

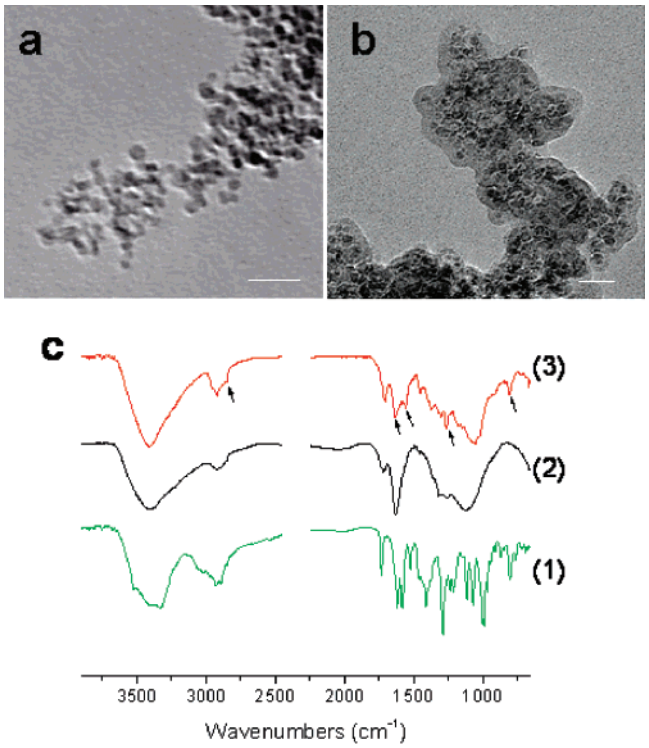

Figure 3. (a,b) Typical TEM images before and after DOX coating, respectively. It can be clearly seen that NDs are coated with another material that is different from pristine NDs in contrast. The thickness of the coated materials is in the range of 2−10 nm. The scale bars are 20 nm. (c) FTIR spectra confirming ND adsorbed with DOX. DOX, NDs, and NDs coated with DOX are shown in Figure c(1−3), respectively. The arrows in Figure 3c indicate the presence of DOX on NDs.

also be demonstrated by the observations provided in the proceeding sections when comparing the activity of the cell cultures in media only, DOX alone upon cell behavior, and DOX−ND composites. While the cells cultured in media alone and drug alone generated a reference (demonstrated quantitatively via MTT assays and DNA fragmentation assays) for drug−ND effects, it could be seen that DOX−ND composites generated an attenuated cell death response that was expected due to the demonstrated drug adsorptive capability of the NDs, confirmed through the NaCl-mediated binding mechanism, TEM imagery, FTIR, and quantitative MTT/DNA fragmentation analysis. Nonbinding between the DOX and NDs would have thus generated an identical effect of cell death (nonattenuated) for the DOX only and DOX−ND conditions. As such, through the several methodologies of verification conducted as detailed above, it could be determined then that the DOX−ND interaction as well as DOX−ND driven cell death was occurring. In addition to surface-bound adsorption of the DOX onto the NDs, the drug that resided within the aggregates due to ND−ND interactions could then have provided a protective or shielding effect for delayed DOX desorption toward transition into slow-release activity so that drug efficacy could potentially be prolonged for translational applications. Furthermore, many chemotherapeutic molecules possess a generalized mechanism of activity such that they act on both healthy and cancerous cells. The ability to shield nonutilized drug molecules from the surrounding environment would then protect against cytotoxic therapeutic activity against unaffected cells. Subsequent studies of functionalizing the ND surfaces with cellular targeting elements (e.g., antibodies, aptamers, etc.) would add another level of intelligence to this carrier technology to drive targeted and slow drug release.[39−42]

Parts a and b of Figure 3 show typical TEM images before and after DOX coating, respectively. It can be clearly seen that the NDs were coated with another material that was different from the pristine NDs in contrast. The thickness of the coated materials was in the range of 2−10 nm. Because no other solid materials except the drug were used, the composition of the coated layer could be reasonably assigned to the drug. This was confirmed by FTIR analysis of the drug-coated NDs. The FTIR peaks, as indicated with the arrows in Figure 3c(3), can be clearly assigned to the drug. For comparison, the FTIR spectrum of pure DOX is shown in Figure 3c(1). In addition to the readily formed ND aqueous suspensions, the hydrogel nature of the NDs can be seen in the rich presence of −OH and −COOH functional groups in the FTIR spectrum, as shown in Figure 3c(2). The amenability of the ND carrier technology with water as a solvent makes it a suitable system for future in vivo testing and facile injection protocols.

Visualization of ND−Cell Interaction. To understand the rate of ND movement into living cells, which is a vital property for the NDs as efficient drug carriers, we first coated fluorescent FITC-linked poly-L-lysine (PL, Sigma) onto the NDs (PL/ND = 10 wt %) via a physical adsorption mechanism analogous to the adsorptive mechanism employed for DOX−ND interfacing and then grew the cells with the fluorescent agent modified NDs. The living cells were fixed in a series of growth periods (0, 1, 3, 5, 10, 24 h) using freshly depolymerized paraformaldehyde (4.0 wt %) in a phosphate buffer (pH = 7.2) and then examined using confocal microscopy. In the confocal images, the NDs were observed to attach to cell membranes instantly, as seen in Figure 4a, in which the fluorescent rings are from PL-coated NDs. Small fluorescent dots (instead of ringlike structures) were visible in the cells fixed at a growth period of 1 h or longer (Figure 4b), indicating that the living cells interact with the NDs dynamically. While it is challenging to determine the exact internalization speed in this dynamic process, many of the fluorescent ND aggregates were found inside the cells within 10 h by *z*-sectional confocal imaging. To visualize the nuclei of the cells grown with the addition of the NDs, we also stained half of the cells with the DNA-binding dye TOTO-1 (T3600, Invitrogen). As shown in Figure 4c, while the NDs were not visible in this case, the clear profile and integrity of the cell nuclei implied that the cell nuclei were not affected by the internalized NDs.

The internalization of the NDs and DOX−ND composites was also examined via TEM. The efficiency of the NDs as a drug carrier was evidenced by the rich presence of ND aggregates inside the cells, as shown in Figure 4f. Although this representative image does not specify the exact location of the ND particles, most of them appeared to localize in

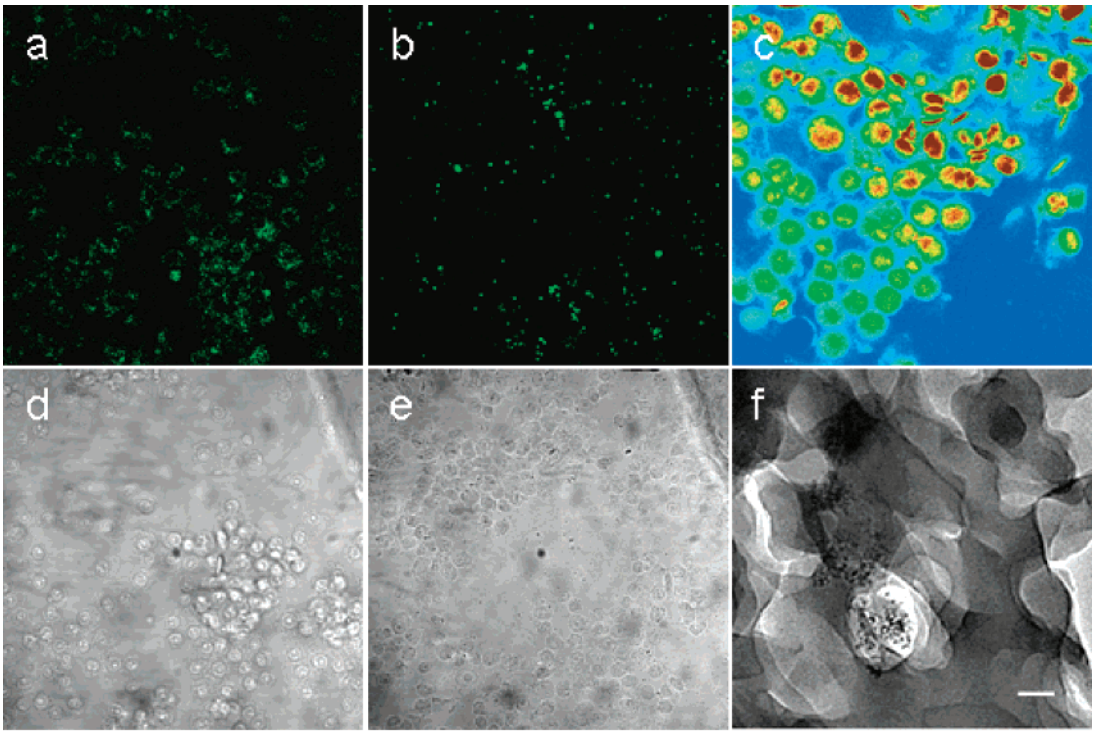

Figure 4. (a−e) Confocal images of macrophage RAW cells with addition of NDs (20 μg/mL) coated with fluorescent poly-L-lysine (FITC-PL/ND ~ 10 wt %). (a,b) Taken from the cells after the addition of NDs without and with incubation (37 °C for 10 h), respectively. The excitation wavelength is 488 nm. (d−e) are bright-field images corresponding to (a) and (b), respectively. (c) From the same cells as in (b) but was stained with dye TOTO-1 and excited with 514 nm laser. The nucleus of the cells can be clearly identified. (f) TEM image showing NDs in macrophage cytoplasm. The image was taken after 3 h incubation of the cells with addition of DOX coated NDs (10 wt %). The cells are dehydrated, fixed, and sliced for TEM observation. The scale bar is 20 nm.

the cytoplasm in aggregates in the range of 50−500 nm in size. Given the loading capabilities of the NDs and the aforementioned notion of DOX integrated within aggregate interiors due to the clustering of ND−DOX particles observed via TEM (Figure 3a,b), it was possible that drug molecules were sequestered within the ND aggregates such that, in addition to the clearly shown surface-adsorbed DOX, the aggregates contained excess and shielded surface-bound DOX not exposed to the ambient environment, which were subsequently introduced into the cells quickly. This was shown by the rapid transmembrane transport capabilities of the NDs and the demonstrated preservation of fluorescent poly l-lysine, which was interfaced with the NDs through a parallel physical mechanism used for DOX adsorption. In addition, some of the drug could also have been released after internalization, and thus the reduction of overall quantity of the drug to achieve the same efficacy could have been anticipated. Compared to free-floating drug administration, if any embedded drug within the ND aggregates was released, a potential mechanism could have been based on gradual desorption. Furthermore, the preservation of poly l-lysine adsorption to the NDs during intracellular trafficking and observation of ND-mediated drug adsorption capabilities verified optically and quantitatively coupled with demonstrated cell death and DNA fragmentation through DOX activity suggest a desorption mechanism of activity. The ability to maintain drug concentrations at a low while effective level over a longer period of time would thus serve as an important parameter of advanced drug delivery systems in the pre-clinical/clinical trial phase.

Examination of Innate Biocompatibility of the ND Delivery System. To determine the biocompatibility of the nanodiamonds for potential use as a material for drug delivery in patients, the cellular response toward incubation with nanodiamonds in culture media was investigated. As a first step to studying the bio-interfacial ND properties, cell viability during growth in culture with the NDs was monitored at 24 and 72 h. Importantly, the response of genes involved in inflammation, which is not examined in conventional cell viability tests, was also assessed.[34] Specifically, interleukin-6 (IL-6), tumor necrosis factor α (TNFα), and inducible nitric oxide synthase (iNOS) expression was evaluated using RT-PCR.[43−45] In addition, the Bcl-x gene was analyzed to examine any effects upon cellular apoptotic behavior/toxicity via ND incubation with the macrophages. Cellular inflammation was chosen as a factor of biocompatibility for several reasons, including the knowledge that inflammation is instrumental in the body for resistance to infection and for the protection from foreign bodies.[46] Chronic inflammation can cause apoptosis in various tissues and even prostate cancer generation,[47,48] thus adding to the danger of implantation or administration of nonbiocompatible materials. While the examination of IL-6, TNFα, iNOS, and Bcl-x elucidates some of the many segments of a broad spectrum of cellular regulatory behavior in response to nanomaterial exposure, the four specific genes that were

selected were adapted to the context of the outlined work in that even though they represent a segment of the collective cellular gene response, they provide important insight into cell response from two perspectives. One perspective serves as an indicator of basal cytokine secretion in the context of examining the translational potential of the material through confirming the lack of evident increases in inflammatory gene expression, which contributes strongly to strengthening the clinical potential of the material. The second perspective addresses the negative complications that have been widely demonstrated/associated with increased basal inflammation and the predisposition/onset/proliferation of cancer, all of which are catalyzed through increased endogenous levels of IL-6, TNFα, and iNOS, for example. More specifically, the absence of ND-mediated up-regulation of cytokine production served as a positive indicator of the ND as a suitable drug delivery material, as increases in endogenous cytokine levels have been shown to play a role in the onset as well as progression of multiple disorders including silencing of chemotherapeutic activity as well as tumor angiogenesis, all of which would serve as counteracting events to the perceived benefits of nanomaterial-mediated drug delivery.

IL-6 is a secreted protein and has been shown to play a significant role in several physiological disorders, including tumor angiogenesis, the protection of tumor cells from the host immune system, as well as inflammation. Its signaling mechanism involves Jak/STAT, Ras/MAP kinase (MAPK), and PI-3 kinase (PI3-K)/Akt pathways that are also inherently correlated with multiple cellular processes including mechanosensation and cancer.[49−53] It has also been observed that the role of IL-6 in cancer processes varies depending on the cell type upon which it acts. For example, IL-6 has been shown to promote the growth of multiple myelomas as well as prostate cancer cells. However, IL-6 has also been shown to inhibit breast cancer as well as lung cancer cells in vivo.[54−56] With specific regard to tumor angiogenesis, IL-6 has been shown to enhance the angiogenic capabilities of cervical tumor cells via downstream up-regulation of vascular endothelial growth factor (VEGF).[57]

IL-6 has also been implicated in the progression of prostate cancer via its secretion mediated by transforming growth factor (TGF)-β1 through multiple signaling pathways including nuclear factor-κB (NF-κB), JNK, and Ras.[58] Elevated serum IL-6 levels have also been correlated with hormone-refractory disease as well as cancer morbidity.[59−62] IL-6 was further shown to serve as a potent autocrine growth factor in vivo for primary, androgen-dependent cancers.[63−65] A key observation with the role of IL-6 in tumor progression/pathogenesis was shown by a preference for prostate cancer cell spreading toward organs that exhibited elevated levels of IL-6 secretion including bone, lymph nodes, and the lungs.[66] In the context of chemotherapeutic delivery, endogenous IL-6 has been shown to confer prostate carcinoma cell resistance toward therapeutic agents, including *cis*-diamminedichloroplatinum and etoposide. As such, the observation that tissue-ND incubation does not induce IL-6 up-regulation displays another level of significance in that favorable nanomaterial−tissue interfacing at the genetic level is critical for the preserved activity of therapeutic systems for which the novel material and delivery were initially engineered.

The significance of the lack of observed increased tumor necrosis factor-alpha (TNF-α) expression via cellular−ND interfacing can be explained by the fact that, while it has been shown to play a role as a marker for cellular inflammation and stress, it also possesses innate relevance to the progression of cancer at elevated levels. For example, TNF-α has been shown to induce cellular DNA damage via reactive ion species.[67] In murine in vivo testing, elevated TNF-α levels were shown to induce oxidative stress and damage to nucleotides, as well as malignant transformation of mouse embryo fibroblasts. TNF-α and its role in chronic inflammatory diseases has been shown to predispose individuals to the onset of cancer development, and its signaling has been correlated with chemically induced skin cancers.[68,69] TNF-α also plays a significant role in inflammation-driven cancer development via NF-κB activation, which in turn supports the viability/inhibits apoptosis of precancerous and transformed cells.[70−73] As such, ND incubation with Raw 264.7 macrophages demonstrated a significant characteristic of the material in that basal TNF-α levels were not elevated, indicating a lack of cellular inflammatory response in vitro. This observation may also provide additional support to the ND as a medically relevant technology given the established adverse downstream effects that elevated TNF-α levels would have elicited.

Inducible nitric oxide synthase (iNOS) has been shown to play a role in tumor progression, angiogenesis, as well as suppression of apoptosis mechanisms by engaging in crosstalk behavior with the COX-2 pathway.[74] As such, a nonelevated iNOS response following cellular−ND interfacing served as another positive aspect of the nonfunctionalized ND as a biocompatible drug carrier system.

Shown in Figure 5a,b are genetic analysis results performed to monitor inflammation of RAW 264.7 murine macrophages upon addition of nanodiamonds at a concentration of 100 μg/mL relative to the culture media at 24 and 72 h after addition. The value of 100 μg/mL was selected in this case as the PCR concentration as it served as the upper limit of the ND concentrations added to the cell lines before excess aggregation of the NDs was observed. The IL-6, iNOS, and TNF-α genes were examined for increased expression as an indicator of inflammation, while Bcl-x was examined for decreased expression, which would have served as an indicator for decreased cellular protection against apoptosis as well as potential cytotoxicity. No inflammation was detected for the three selected cytokines we examined, as expression levels were not significantly up-regulated following ND incubation and Bcl-x expression was not decreased, indicating that the NDs are biocompatible at the genetic level in vitro. While any nanomaterial-induced enhancement in IL-6, TNF-α, iNOS, or decreases in Bcl-x expression would clearly not be correlated to the onset of cancer necessarily, increased levels of the inflammatory regulatory molecules in the body can clearly play a relevant role in the activation of signaling elements that can in turn

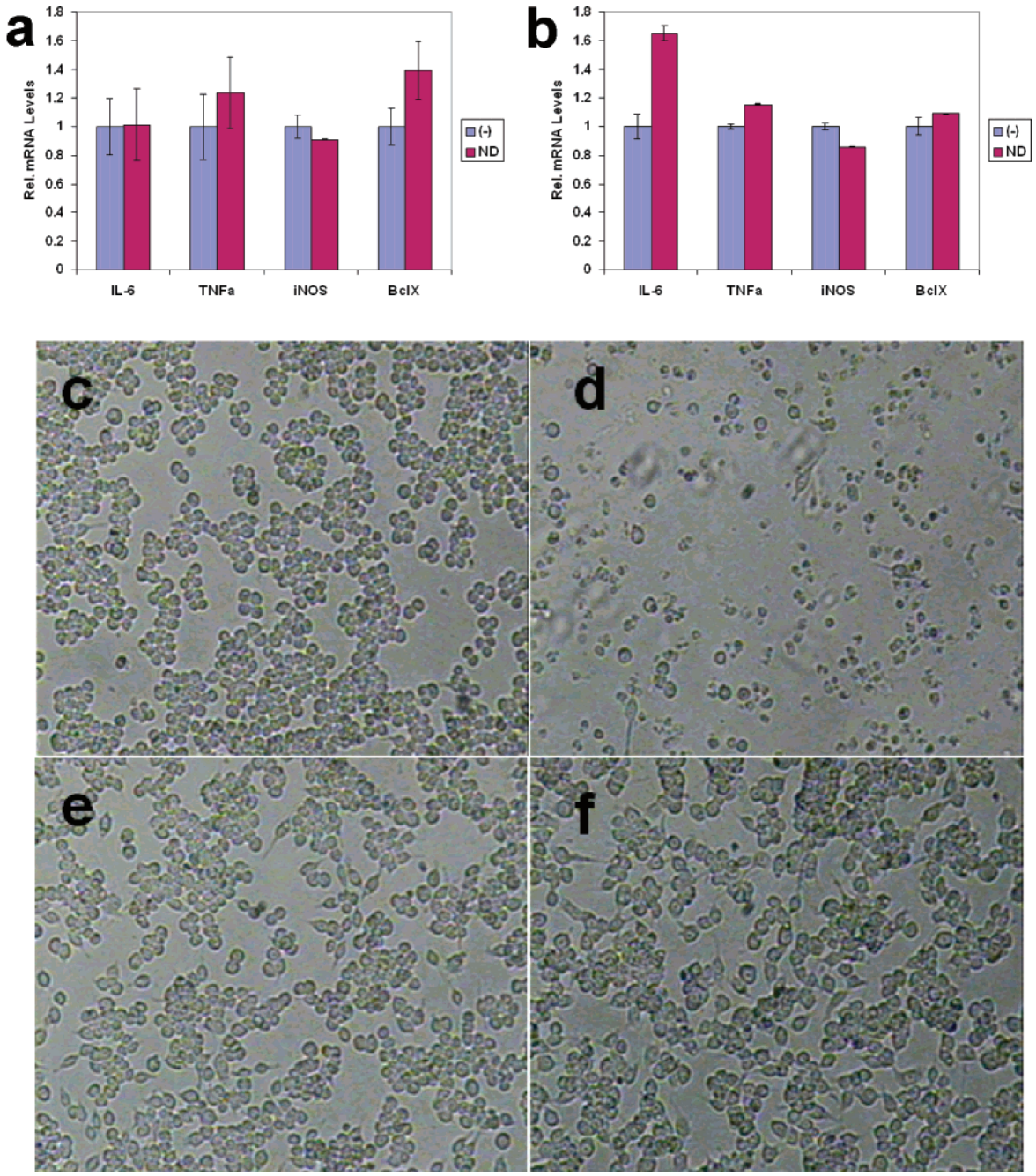

Figure 5. (a) Genetic analysis (real-time PCR) was performed to monitor inflammation and apoptotic response of RAW 264.7 murine macrophage upon addition of nanodiamonds (100 μg/mL, 24 h growth). The inflammation genes studied included iNOS, TNFα, and IL-6. Bcl-x was also studied, and the lack of decrease in expression levels were indicative of a nonapoptotic cell response to the bare NDs. (b) PCR was also performed at a 72 h time point for the macrophages, which indicated a similar cellular response and favorable bio-interfacial properties of the NDs in the context of both inflammation and apoptosis in vitro. In addition to the optical studies of cellular response to the NDs and DOX−ND composites, the biological amenability of the NDs, DOX-induced cell death, as well as DOX−ND induced cell death were confirmed via DNA fragmentation as well as MTT assays. For the optical/morphological analysis of drug-induced effects upon the RAW 265.7 murine macrophages, the cells were cultured for 24 h and morphologies were monitored via optical microscopy. (c) Cell morphologies in media only and density were observed which indicated normal cell morphology and density, (d) Cells cultured in the presence of DOX resulted in widespread cell death, as shown by significantly decreases in cell density and abnormal morphology of remaining debris (3 μg/mL DOX). (e) Cells cultured with bare nanodiamonds resulted in the morphologies and densities similar to those observed with cells cultured in media only (30 μg/mL NDs), and (f) cells cultured with DOX−ND complexes resulted in ND-induced sequestering of DOX and reduced cell death, which was further confirmed via MTT and DNA fragmentation assays. (30 μg/mL ND + 3 μg/mL DOX) (Leica Lambda DG-4, magnification × objective: (40 × 10)).

result in adverse physiological reactions. Furthermore, a key element of advanced chemotherapy mediated by these novel nanodiamond systems rests with their ability to maintain steady levels of cytokines such that secondary effects due to ND presence are not activated. As cytokine up-regulation has been implicated in physiological disorders that extend well beyond cancer progression, the absence of IL-6, TNFα, and iNOS up-regulation or a Bcl-x expression decrease

following cellular incubation with the NDs demonstrates its innate potential for biocompatible drug delivery.

DOX−ND-Induced Cellular Apoptosis. Interactions of bare NDs and the macrophages, as well as the DOX−ND composites and macrophages, were imaged by optical microscopy and morphological analysis was performed to assess DOX−ND effects and impact upon cellular morphology/architectures. This visual/morphological assessment was then supported by substantial further testing that provided quantitative support of several factors, including the innate biocompatibility of the NDs, DOX−ND efficacy in multiple cell lines (Raw 264.7 and HT-29), DOX-only efficacy, and LPS-inhibited DOX activity (conditions assessed via RT-PCR, MTT assays, DNA fragmentation assays). Cell imagery and visual analysis were conducted 18 h postincubation under the given parameters. In Figure 5c, the macrophages cultured in media only resulted in standard morphologies and density/viability, which was previously confirmed via MTT/DNA fragmentation. In Figure 5d, it could clearly be seen that both cellular morphology as well as the absence of the cells bearing a normal morphology as shown in Figure 5c were correlated with the addition of pure DOX, which was also confirmed from the MTT/DNA fragmentation assays (3 μg/mL DOX). In Figure 5e, ND-only incubation also showed a clear distinction from Figure 5d, as the cell bodies possessed morphologies similar to Figure 5c that were indicative of healthy growth, and ND bio-amenability was again confirmed via MTT/DNA fragmentation assays (30 μg/mL NDs). Figure 5f confirmed an attenuated effect of the DOX−NDs upon the cells, which was expected due to the adsorptive effects of the NDs upon the DOX and subsequent reduction in DOX-mediated effects upon cellular morphology, with impact upon cell death also confirmed by the MTT/DNA fragmentation assays (30 μg/mL NDs + 3 μg/mL DOX).

To further examine and confirm that cell death upon addition of the DOX−ND composites is DOX-induced activation of apoptosis, studies of LPS-mediated effects upon DOX activity were also conducted where cells were pretreated with lipopolysaccharide (LPS, 10ng/mL), a known inhibitor of DOX-mediated apoptosis, and then DOX−ND composites were added.[75] Cell death in the presence of the same additives as shown in Figure 5d was significantly decreased (Supporting Information Figure 1). Apoptotic cells exhibit a number of characteristic phenotypes, including damage and fragmentation of cellular DNA, activation of caspase-3 (a mediator of apoptosis), and the cleavage of poly-(ADP-ribose) polymerase. Previous studies have demonstrated the progression of these three apoptosis signals upon the treatment of murine macrophage cells with DOX.[75] Inflammatory pathway activation has previously been shown to be a potent blocker of DOX-mediated cell death. The stimulation of inflammation involves the induction of gene expression from a number of loci, including IL-6. Overexpression of IL-6 has also been shown to inhibit p53-mediated apoptosis.[76,77] As LPS is a bacterial cell membrane component that induces inflammation in macrophage cells, and consistent with previous inflammation-mediated apoptotic preclusion, LPS pretreatment of macrophage cells was shown to inhibit DOX (released from NDs) induced apoptosis.

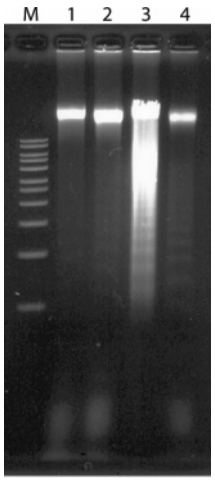

Figure 6. Electrophoreses of DNA extracted from RAW 264.7 murine macrophage cells alone (lane 1) in the presence of nanodiamonds (25 μg/mL, lane 2), doxorubicin (2.5 μg/mL, lane 3), and nanodiamonds conjugated with doxorubicin (25 μg/mL ND + 2.5 μg/mL DOX, lane 4). DNA was isolated via gentle cell lysis and RNase and ProteinaseK treatment followed by phenol chloroform extraction and isopropanol precipitation. The fragmentation of DNA is indicative of cell death due to apoptosis. The addition of doxorubicin (lane 3) leads to a significant increase in cell death, and the addition of nanodiamonds with doxorubicin (lane 4) significantly attenuates this cell death. All cells were cultured for 18 h prior to harvest.

DNA Assay for DOX−ND Composite Driven Cell Death. Because the fragmentation of cellular DNA is indicative of apoptotic cell death, the different extent of cell death induced by free-floating DOX and DOX−ND composites can be examined via gel electrophoresis of fragmented DNA. Shown in Figure 6 are comparative DNA assays of DOX−ND activity at 18 h. Because the NDs are innately biocompatible, as demonstrated in the PCR studies as mentioned before, lane 2 served as the control. As seen in lane 2, no DNA fragmentation was observed and thus bare NDs did not induce cellular apoptosis. DNA fragmentation could be seen in cells grown with the addition of free-floating DOX (lane 3). The addition of the NDs with the DOX significantly decreased the amount of DNA fragmentation (lane 4). The effects of the NDs on DOX-induced cell death could be clearly seen because the amounts of DOX added in these two samples were identical. As previously stated, the attenuated effect of the DOX−ND composites and their generation of gradual cell death were expected due to the demonstrated drug adsorptive capability of the NDs, confirmed through the NaCl-mediated mechanism, TEM imagery, FTIR, and quantitative MTT/DNA fragmentation analysis. Nonbinding between the DOX and NDs would have resulted in the identical potency of cell death in the form of observed fragmentation (e.g., nonattenuated) for the DOX only and DOX−ND conditions because the same amount of drug would have been acting on the cells due to the equal amounts added to the DOX only and DOX−ND solutions (3 μg/mL). On the contrary, however, to further confirm the TEM imagery and MTT data observed, the DNA fragmenta-

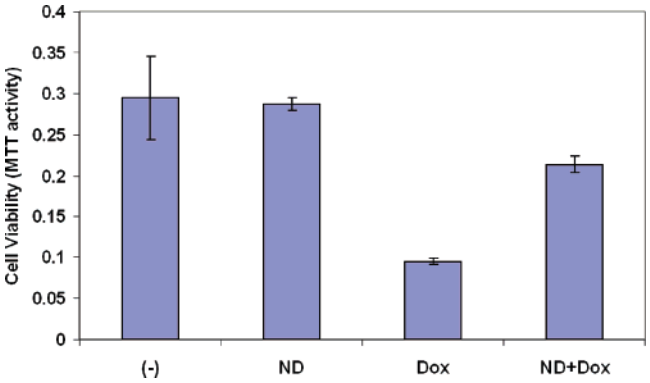

Figure 7. Cell viability assay (MTT based) of HT-29 human colorectal adenocarcinoma cells (ATCC) grown alone (−), with 25 μg/mL nanodiamonds (ND), with 2.5 μg/mL doxorubicin (DOX), or with 25 μg/mL nanodiamonds conjugated with 2.5 μg/mL doxorubicin (ND + DOX). All samples done in triplicate.

tion pattern observed for the DOX−ND composites were then expectedly displayed through the ND modulation of drug sequestering that resulted in gradual cell death via DOX activity. As such, through the several methodologies of verification conducted as detailed above, it could be determined then that the DOX−ND interaction as well as DOX−ND driven cell death was occurring. In addition, longer cellular incubation with DOX−ND composites led to progression of apoptotic cell death, which also demonstrated a functional element of the DOX−ND composites (data not shown). The relative cell viability with the three different added components, which is reflected in the fragmented DNA patterns, is as follows: NDs > DOX−ND > DOX. This result is consistent with the cell morphology changes observed previously via optical microscopy.

MTT Assay of DOX−ND Activity in the HT-29 Colorectal Cancer Cell Line. To explore the platform capabilities of the ND drug-carrying technology, we also applied the DOX−ND composites toward the HT-29 human colorectal cancer cell line. MTT-based cell viability assays were done using HT-29 human colorectal adenocarcinoma cells (ATCC) (Figure 7). Cells were seeded at ∼40% confluency in McCoy's 5A media supplemented with 10% fetal bovine serum. Nanodiamonds were added to the cells at a final concentration of 25 μg/mL, doxorubicin at a concentration of 2.5 μg/mL, or a mixture of nanodiamonds and doxorubicin at concentrations of 25 and 2.5 μg/mL, respectively. Cells were grown for 41 h at 37 °C with 5% CO_2, and the cell viability assay was performed following the manufacturer's protocol (Sigma-Aldrich) and read in a Safire multiwell plate reader (Tecan) using Magellan software (Tecan) for analysis. Samples were done in triplicate. No difference was seen in cell viability when cells were grown in the presence of nanodiamonds, which further confirmed the biocompatibility of the NDs. Doxorubicin significantly decreased cell viability, as expected with this lane, serving as the reference for the DOX−ND composite effects upon HT-29 viability. It was then shown that, following the addition of the composites, the effect of the doxorubicin was attenuated through ND-mediated DOX sequestering. As such, this study further extended the applicability of the DOX−NDs from the model RAW 264.7 murine macrophage, which served as a testing platform for both drug−ND efficacy as well as innate biocompatibility, toward a more clinically relevant colorectal cancer cell line to demonstrate the translational potential of this technology.

Summary. We have demonstrated that nanodiamonds serve as concentration-tuning substrates that can be interfaced with a chemotherapeutic drug while further serving as stabilization matrices to preserve drug functionality. Doxorubicin hydrochloride (DOX), an apoptosis-inducing drug widely used in chemotherapy, was successfully and reversibly coated on the nanodiamonds materials (NDs, 2−8 nm) and introduced into living cells. The adsorption of DOX onto the NDs and its reversible release were achieved by regulating Cl^- ion concentration to elucidate the potential of switchable drug elution mediated at the ND surface. Following the observation of efficient ND-driven drug internalization, comprehensive bioassays were performed to assess and confirm the innate biocompatibility of the NDs and stable gene program activity via RT-PCR. Genetic and viability interrogation were applied toward the observation of functional apoptosis-inducing mechanisms enabled by the DOX-functionalized ND composite materials, confirming its applicability as a platform transport technology for a multitude of therapeutic molecules and broad nanoscale medicine modality.

Acknowledgment. We gratefully acknowledge the support of grant U54 A1065359 from the National Institute of Allergy and Infectious Diseases of the National Institutes of Health.

Supporting Information Available: LPS-mediated confirmation of DOX-induced cell death. This material is available free of charge via the Internet at http://pubs.acs.org.

References

(1) Langer, R.; Tirrell, D. A. *Nature* **2004**, *428*, 487−492.
(2) Langer, R. *Nature* **1998**, *392*, 5−10.
(3) Allen, T. M.; Cullis, P. R. *Science* **2004**, *303*, 1818−1822.
(4) Niemeyer, C. M. *Angew. Chem., Int. Ed.* **2001**, *40*, 4128−4158.
(5) Rao, C. N. R.; Cheetham, A. K. *J. Mater. Chem.* **2001**, *11*, 2887−2894.
(6) Caruso, F. *Adv. Mater.* **2001**, *13*, 11−22.
(7) Gao, X. H.; Cui, Y. Y.; Levenson, R. M.; Chung, L. W. K.; Nie, S. M. *Nat. Biotechnol.* **2004**, *22*, 969−976.
(8) Moghomi, S. M.; Hunter, A. C.; Murray, J. C. *Pharm. Rev.* **2001**, *53*, 283−318.
(9) Shinohara, H. Rep. *Prog. Phys.* **2000**, *63*, 843−892.
(10) Nakamura, E.; Isobe, H. *Acc. Chem. Res.* **2003**, *36*, 807−815.
(11) Sun, Y. P.; Fu, K. F.; Lin, Y.; Huang, W. J. *Acc. Chem. Res.* **2002**, *35*, 1096−1104.
(12) Lin, Y.; Tayor, S.; Lin, H. P.; Fernando, K. A. S.; Qu, L. W.; Wang, W.; Gu, L. R.; Zhou, B.; Sun, Y. P. *J. Mater. Chem.* **2004**, *14*, 527−541.
(13) Bianco, A.; Kostarrelos, K.; Partidos C. D.; Prato, M. *Chem. Commun.* **2005**, 571−577.
(14) Chen, X.; Tam, U. C.; Czlapinski, J. L.; Lee, G. S.; Rabuka, D.; Zettle, A.; Bertozzi, C. R. *J. Am. Chem. Soc.* **2006**, *128*, 6292−6293.
(15) Bianco, A.; Prato, M. *Adv. Mater.* **2003**, *15*, 1765−1768.
(16) Manna, S. K.; Sarkar, S.; Barr, J.; Wise, K.; Barrera, E. V.; Jejelowo, O.; Rice-Ficht, A. C.; Ramesh, G. T. *Nano Lett.* **2005**, *5*, 1676−1684.
(17) Lacerda, L.; Bianco, A.; Prato, M.; Kostarelos, K. *Adv. Drug Delivery Rev.* **2006**, *58*, 1460−1470.

(18) Oberdorster, E. *Environ. Health Perspect.* **2004**, *11*, 1058−1062.
(19) Warheit, D. B.; Laurence, B. R.; Reed, K. L.; Roach, D. H.; Reynolds, G. A. M.; Webb, T. R. *Toxicol. Sci.* **2004**, *77*, 117−125.
(20) Jia, G.; Wang, H. F.; Tan, L.; Wang, X.; Pei, R. J.; Yan. T.; Zhao, Y. L.; Guo, X. B. *Environ. Sci. Technol.* **2005**, *39*, 1378−1383.
(21) Smart, S. K.; Cassady, A. I.; Lu, G. Q.; Martin, D. J. *Carbon* **2006**, *44*, 1034−1047.
(22) Kam, N. W. S.; Jessop, T. C.; Wender, P. A.; Dai, H. J. *J. Am. Chem. Soc.* **2004**, *126*, 6850−6851.
(23) Kam, N. W. S.; Dai, H. J. *J. Am. Chem. Soc.* **2005**, *127*, 6021−6026.
(24) Pantarotto, D.; Briand, J. P.; Prato, M.; Bianco, A. *Chem. Commun.* **2004**, 16−17.
(25) Pantarotto, D.; Singh, R.; McCarthy, D.; Erhardt, M.; Briand, J. P.; Prato, M.; Kostarelos, K.; Bianco, A. *Angew. Chem. Intl. Ed.* **2004**, *43*, 5242−5246.
(26) Cai, D.; Mataraza, J. M.; Qin, Z. H.; Huang, Z. P.; Huang, J. Y.; Chiles, T. C.; Carnahan, D.; Kempa, K.; Ren, Z. F. *Nat. Methods* **2005**, *2*, 449−454.
(27) Kam, N. W. S.; O'Connell, M.; Wisdom, J. A.; Dai, H. J. *Proc. Natl. Acad. Sci.* **2005**, *102*, 11600−11605.
(28) Manna, S. K.; Sarkar, S.; Barr, J.; Wise, K.; Barrera, E. V.; Jejelowo, O.; Rice-Ficht, A. C.; Ramesh, G. T. *Nano Lett.* **2005**, *5*, 1676−1684.
(29) Narayan, R. J.; Wei, W.; Jin, C.; Andara, M.; Agarwal, A.; Gerhardt, R. A.; Shih, C. C.; Shih, C. M.; Lin, S. J.; Su, Y. Y.; Ramamurti, Y.; Singh, R. N. *Diamond Relat. Mater.* **2006**, *15*, 1935−1940.
(30) Yu, S. J.; Kang, M. W.; Chang, H. C.; Chen, K. M.; Yu, Y. C. *J. Am. Chem. Soc.* **2005**, *127*, 17604−17605.
(31) Fu, C. C.; Lee, H. Y.; Chen, K.; Lim, T. S.; Wu, H. Y.; Lin, P. K.; Wei, P. K.; Tsao, P. H.; Chang, H. C.; Fann, W. *Proc. Natl. Acad. Sci. U.S.A.* **2007**, *104*, 727−732.
(32) Greiner, N. R.; Phillips, D. S.; Johnson, J. D.; Volk, F. *Nature* **1988**, *333*, 440−442.
(33) Kruger, A.; Kataoka, F.; Ozawa, M.; Fujino, T.; Suzuki, Y.; Alesenskii, A. E.; Vul, A. Y.; Osawa, E. *Carbon* **2005**, *43*, 1722−1730.
(34) Schrand, A. M.; Huang, H. J.; Carlson, C.; Schlager, J. J.; Osawa, E.; Hussain, S. M.; Dai, L. *J. Phys. Chem. B* **2007**, *111*, 2−7.
(35) Huang, L. C. L.; Chang, H. C. *Langmuir* **2004**, *20*, 5879−5884.
(36) Chung, P. H.; Perevedentseva, E.; Tu, J. S.; Chang, C. C.; Cheng, C. L. *Diamond Relat. Mater.* **2006**, *15*, 622−625.
(37) Nguyen, T. T. B.; Chang, H. C.; Wu, V. W. K. *Diamond Relat. Mater.* **2007**, *16*, 872−876.
(38) Ozawa, M.; Inaguma, M.; Takahashi, M.; Kataoka, F.; Krüger, A.; Osawa, E. *Adv. Mater.* **2007**, *19*, 1201.
(39) Dachs, G. U.; Dougherty, G. J.; Stratford, I. J.; Chaplin, D. J. *Oncol. Res.* **1997**, *9*, 313−325.
(40) Portney, N. G.; Ozkan, M. *Anal. Bioanal. Chem.* **2006**, *384*, 620−630.
(41) Farokhzad, O. C.; Jon, S.; Khademhosseini, A.; Tran, T. T.; LaVan, D. A.; Langer, R. *Cancer Res.* **2004**, *64*, 7668−7672.
(42) Farokhzad, O. C.; Cheng, J. J.; Teply, B. A.; Sherifi, I.; Jon, S.; Kantoff, P. W.; Richie, J. P.; Langer, R. *Proc. Natl. Acad. Sci. U.S.A.* **2006**, *103*, 6315−6320.
(43) Heinrich, P. C.; Behrmann, I.; Haan, S.; Hermanns, H. M.; Muller-Newen, G.; Schaper, F. *Biol. Chem. J.* **2003**, *374*, 1−20.
(44) MacEwan, D. J. *Cell. Signalling* **2002**, *14*, 477−492.
(45) Aktan, F. *Life Sci.* **2004**, *75*, 639−653.
(46) Boehm, U.; Klamp, T.; Groot, M.; Howard, J. C. *Annu. Rev. Immun.* **1997**, *15*, 749−795.
(47) Hjelmstrom, P. *J. Leukocyte Biol.* **2001**, *69*, 331−339.
(48) Palapattu, G. S.; Sutcliffe, S.; Bastian, P. J.; Platz, E. A.; De Martzo, A. M.; Isaacs, W. B.; Nelson, W. G. *Carcinogenesis* **2005**, *26*, 1170−1181.
(49) Taga, T.; Kishimoto, T. *Annu. Rev. Immunol.* **1997**, *15*, 797−819.
(50) Willenberg, H. S.; Päth, G.; Vögeli, T. A.; Scherbaum, W. A.; Bornstein, S. R. *Ann. N. Y. Acad. Sci.* **2002**, *966*, 304−14.
(51) Kishimoto, T.; Akira, S.; Narazaki, M.; Taga, T. *Blood* **1995**, *86*, 1243−1254.
(52) Murakami, M.; Hibi, M.; Nakagawa, N.; Nakagawa, T.; Yasukawa, K.; Yamanishi, K.; Taga, T.; Kishimoto T. *Science* **1993**, *260*, 1808−1810.
(53) Hirano, T.; Nakajima, K.; Hibi, M. *Cytokine Growth Factor Rev.* **1997**, *8*, 241−252.
(54) Danforth J. D. N.; Sgagias, M. K. *Cancer Res.* **1993**, *53*, 1538−1545.
(55) Klein, B.; Zhang, X. G.; Lu, Z. Y.; Bataille, R. *Blood* **1995**, *85*, 863−872.
(56) Okamoto, M.; Lee, C.; Oyasu, R. *Cancer Res.* **1997**, *57*, 141−146.
(57) Wei, L. H.; Kuo, M. L.; Chen, C. A.; Chou, C. H.; Lai, K. B.; Lee, C. N.; Hsieh, C. Y. *Oncogene* **2003**, *22*, 1517−1527.
(58) Park, J. I.; Lee, M. G.; Cho, K.; Park, B. J.; Chae, K. S.; Byun, D. S.; Ryu, B. K.; Park, Y. K.; Chi, S. G. *Oncogene* **2003**, *22*, 4314−4332.
(59) Adler, H. L.; McCurdy, M. A.; Kattan, M. W.; Timme, T. L.; Scardino, P. T.; Thompson , T. C. *J. Urol.* **1999**, *161*, 182−187.
(60) Drachenberg, D. E.; Elgamal, A. A.; Rowbotham, R.; Peterson, M.; Murphy, G. P. *Prostate* **1999**, *41*, 127−133.
(61) Twillie, D. A.; Eisenberger, M. A.; Carducci, M. A.; Hsieh, W. S.; Kim, W.Y.; Simons, J. W. *Urology* **1995**, *45*, 542−549.
(62) Siegsmund, M. J.; Yamazaki, H.; Pastan, I. *J. Urol.* **1994**, *151*, 1396−1399.
(63) Giri, D.; Ozen, M.; Ittmann, M. *Am. J. Pathol.* **2001**, *159*, 2159−2165.
(64) Qiu, Y.; Robinson, D.; Pretlow, T. G.; Kung, H. J. *Proc. Natl. Acad. Sci. U.S.A.* **1998**, *95*, 3644−3649.
(65) Deeble, P. D.; Murphy, D. J.; Parsons, S. J.; Cox, M. E. *Mol. Cell. Biol.* **2001**, *21*, 8471−8482.
(66) Siegall, C. B.; Schwab, G.; Nordan, R. P.; FitzGerald, D. J.; Pastan, I. *Cancer Res.* **1990**, *50*, 7786−7788.
(67) Yan, B.; Wang, H.; Rabbani, Z. N.; Zhao, Y.; Li, W.; Yuan, Y.; Li, F.; Dewhirst, M.; Li, W. *Cancer Res.* **2006**, *66*, 11565−11570.
(68) Hendrickse, C. W.; Kelly, R. W.; Radley, S.; Donovan, I. A.; Keighley, B.; Neoptolemos, J. P. *Br. J. Surg.* **1994**, *81*,1219−1223.
(69) Cianchi, F.; Cortesini, C.; Bechi, P. *Gastroenterology* **2001**, *121*, 1339−47.
(70) Gullino, P. M. *Acta Oncol.* **1995**, *34*, 439−441.
(71) Pai, R.; Szabo, I. L.; Soreghan, B. A.; Atay, S.; Kawanaka, H.; Tarnawski, A. S. *Biochem. Biophys. Res. Commun.* **2001**, *286*, 923−928.
(72) Ziche, M.; Morbidelli, L.; Choudhuri, R. *J. Clin. Invest.* **1997**, *99*, 2625−2634.
(73) Sugimoto, Y.; Narumiya, S.; Ichikawa, A. *Prog. Lipid Res.* **2000**, *39*, 289−314.
(74) Cianchi, F.; Cortesini, C.; Fantappie, O.; Messerini, L.; Sardi, I.; Lasagna, N.; Perna, F.; Fabbroni, V.; Di Felice, A.; Perigli, G.; Mazzanti, R.; Masini, E. *Clin. Cancer Res.* **2004**, *10*, 2694−2704.
(75) Hassan, F.; Islam, S.; Mu, M. M.; Ito, H.; Koide, N.; Mori, I.; Yoshida, T.; Yokochi, T. *Mol. Cancer Res.* **2005**, *3*, 373−379.
(76) Lotem, J.; Gal, H.; Kama, R.; Amariglio, N.; Rechavi, N.; Domany, E.; Sachs, L.; Givol, D. *Proc. Natl. Acad. Sci. U.S.A.* **2003**, *100*, 6718−6723.
(77) Duan, Z.; Lamendola, D. E.; Penson, R. T.; Kronish, K. M.; Seide, M. V. *Cytokine* **2002**, *17*, 234−242.

NL071521O